Journal of New Materials for Electrochemical Systems 14, 011-017 (2011)

Corrosion Resistance and Stability of the Pt-Ni and Pt-Co Nanoparticles Prepared by the Double Potential Step Electrolysis

Takashi Nishimura[1,*], Tsutomu Morikawa[1], Masayuki Yokoi[1] and Hiroshi Inoue[2]

[1]Technology Research Institute of Osaka Prefecture, 2-7-1 Ayumino, Izumi, Osaka 594-1157, Japan
[2]Department of Applied Chemistry, Graduated School of Engineering, Osaka Prefecture University, 1-1gakuencho, Sakai, Osaka 599-8531, Japan

Received: September 08, 2010, Accepted: November 10, 2010, Available online: December 20, 2010

Abstract: *The Pt-Ni and Pt-Co nanoparticles covered with a Pt skin layer were prepared by the double potential step electrolysis (DPSE), which composed of potential steps for electrodeposition of the Pt-Ni and Pt-Co alloy and the following selective dissolution of the Ni and Co component, respectively. With this method, the Pt alloy nanoparticles covered with a Pt skin layer could be prepared just in one process, and the composition and size of the Pt alloy nanoparticles could be easily controlled by changing the electrode potential and plating bath composition.*

Both the nanoparticles by the DPSE exhibited higher corrosion resistance and oxygen reduction reaction (ORR) activity than the Pt nanoparticles even after deterioration test, and the surface contents of them were kept constant around 4 % Co and 8 % Ni measured by XPS over the wide range of Pt alloy compositions, respectively. Comparing the Pt-Ni with Pt-Co nanoparticles, the Pt-Co nanoparticles were found to be more stable than the Pt-Ni nanoparticles, and suggested that a Pt-skin layer on Pt alloy particles had an important role in their performances.

Keywords: potential step electrolysis, Pt alloy, nanoparticles, corrosion resistance, stability

1. INTRODUCTION

The alloying of Pt with transition metals such as Co, Ni, Fe etc. gives higher electrocatalytic activity for oxygen reduction reaction (ORR) than pure Pt [1-8, 10-14]. The ORR activity of the Pt-based alloys can be influenced by the shortening of Pt-Pt interatomic distance [7], and the increase in the d-electron vacancy of Pt [8] etc. With an increase in d-electron vacancy of Pt, electron donation from the adsorbed oxygen molecules to Pt atoms increases, leading to weaker O-O bonding and stronger Pt-O bonding. But, too much d-electron vacancy of Pt lowers ORR activity because of too strong Pt-O bonding. Therefore, Pt-based alloys with appropriate d-electron vacancy of Pt have the maximum ORR activity.

It is well-known that transition metal components in Pt-based alloys preferentially dissolve out in acidic solutions during electrochemical operations. So, the durability of Pt-based alloys should be also discussed as a function of the content of transition metal components and surface structure of the alloys.

Bonakdarpour et al. [9] studied the dissolution of Fe and Ni components in $Pt_{1-x}M$ (M=Fe, Ni; $0<x<1$) catalysts, which were prepared by sputtering, in 0.3 or 1 M H_2SO_4 and 0.3 or 1 M $HClO_4$. They demonstrated with energy dispersive spectrometer and X-ray diffraction data that at $x<0.6$ the surface Fe and Ni components preferentially dissolved out, while at $x>0.6$ both surface and bulk ones dissolved. In addition, X-ray photoelectron spectroscopic data demonstrated that both components were not detected at the catalyst surface after the acid treatment. Other researchers also reported the surface transition metal components of Pt-based alloys completely disappeared in almost cases [8, 10]. The preferential dissolution of transition metals from Pt-based alloys caused negative effects such as the lowering of ORR activity [11], the decrease in electrochemical surface area [12] and so on. Hector et al. found that there was a close correlation between the amount of the dissolved metal components and the decrease in ORR activity for the Pt-based alloy catalysts [11]. Travitsky et al. concluded that the corrosion of the transition metal components caused increased

*To whom correspondence should be addressed: Email: t_nishimura@tri.pref.osaka.jp

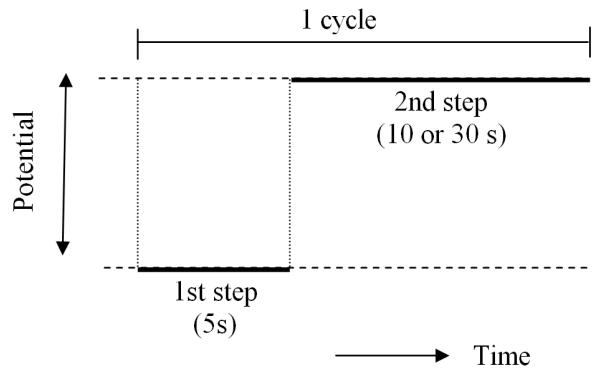

Figure 1. Typical potential step pattern of a cycle of DPSE. The duration of the 1st step was 5 s and the 2nd step, either 10 or 30 s.

grain size of Pt and decreased electrochemical surface area (ECSA) [12]. In PEM fuel cell systems, transition metal ions dissolved out from Pt alloy catalysts would redeposit somewhere else in the cell, leading to the degradation of cell performances.

There have been some attempts [10-12] to prepare Pt-based alloy catalysts with a Pt skin layer which was formed in advance to prevent transition metals from leaching. The Pt-based alloys as a core can be protected from acid solutions by the stable Pt skin layer as a shell. The Pt skin layer had higher stability than the pure Pt due to the electronic effect of underlying alloys [15, 16]. The Pt skin layer is formed by annealing of the Pt-based alloy nanoparticles [17, 18], replacement of a UPD Cu monolayer on a core particle with Pt [19], and the electrochemical stabilization treatment [10]. However, all these methods are two-step processes which are composed of the preparation of Pt-based alloy particles and the following treatment for the Pt skin layer formation. Therefore, simpler technique for the Pt skin layer formation is desirable.

A double potential step electrolysis (DPSE) we have developed previously [20] is a novel preparation method of Pt-Ni nanoparticles covered with a Pt skin layer. With this method, desired composition and size of Pt-Ni alloy nanoparticles could be easily obtained in one process by selecting appropriate electrode potential for the DPSE and plating bath composition. And the resultant nanoparticles exhibited higher ORR activity and corrosion resistance than Pt nanoparticles in acid solution. Recent studies about fuel cell cathode electrocatalysts are mostly focused on Pt-Co nanoparticles, so it is important to apply the DPSE to Pt-Co nanoparticles.

In this paper Pt-Co nanoparticles with a Pt skin layer were prepared by the DPSE. And the electrochemical stability and the corrosion resistance of the resultant Pt-Co nanoparticles were investigated as a function of the alloy composition with repetitive wide potential cycling and XPS measurement and compared with those of the Pt-Ni nanoparticles.

2. EXPERIMENTAL

The Pt-Ni and Pt-Co nanoparticles with different compositions were prepared on a glassy carbon (GC) disc or plate by the DPSE. Typical DPSE is composed of potential steps for the electrodeposition of Pt alloy for 5 s (1st step) and the following selective dissolution of the transition metal for 10 or 30 s (2nd step), as shown in Fig. 1. The 2nd step was performed for complete dissolution of the Ni and Co components from the surface of the nanoparticles. All deposits in this study were prepared by a cycle of the DPSE. The counter and reference electrodes were Pt wire and the Ag/AgCl electrodes, respectively. Electrode potentials measured against the Ag/AgCl electrode were transformed into those against the reversible hydrogen electrode (RHE). Plating baths for Pt-Ni and Pt-Co depositions were based on Watt's nickel bath, composed of 0.91 M $MSO_4 \cdot 6H_2O$, 0.19 M $MCl_2 \cdot 6H_2O$, 0.49 M H_3BO_4, and 1.25, 2.5, 5.0, 10 or 20 mM $H_2PtCl_6 \cdot 6H_2O$ (M = Ni or Co). Each plating bath was called a Pt-Ni bath and Pt-Co bath, respectively. Plating baths without $PtCl_6^{2-}$ were called a Ni bath and Co bath, respectively. For the Pt deposition, 2.5 mM H_2PtCl_6 aqueous solution was used. Detailed information on the DPSE can be found in our previous paper [20].

For evaluating ORR activities of Pt-Ni and Pt-Co nanoparticles-deposited GC discs, hydrodynamic voltammograms were recorded with a rotating disc electrode system at rotation speeds from 400 to 2500 rpm in an O_2-saturated 0.1 M sulfuric acid solution at 30 ^oC. Each voltammogram was measured in the potential range between 0 and 1.0 V at a scan rate of 1mV s^{-1}. Kinetically controlled current (i_k) was evaluated from Koutecky-Levich plots.

The stability of Pt-Ni and Pt-Co nanoparticles catalysts was evaluated from the change in real surface area with potential cycling. The real surface area was evaluated by integrating the oxidation peaks due to atomic hydrogen desorption. Corrosion resistance was evaluated from the change in surface Ni or Co content with potential cycling in an N_2-saturated 0.1 M sulfuric acid solution at 30 ^oC. Potential cycling was performed over the potential range between 0.05 V and 1.2 V at a scan rate of 100 mV s^{-1}.

The surface compositions of Pt-Ni and Pt-Co nanoparticles were evaluated by X-ray photoelectron spectroscopy (XPS). The data were collected with a monochromatic Al K_α radiation. A gold wire was fixed on each sample and Au 4f spectra were measured together with Pt 4f and Ni or Co 2p spectra for calibration of binding energy. The bulk compositions of the Pt-Ni and Pt-Co nanoparticles were evaluated by XPS after Ar^+ sputtering for 0.3 min. The sputtering rate was about 2 nm / min for oxide layer of SiO_2. Particle size and surface morphology of the Pt-Ni and Pt-Co nanoparticles were observed by transmission electron microscopy (TEM). The Pt-Ni and Pt-Co nanoparticles were fixed on Cu mesh with collodion membrane for TEM specimens. The nanoparticles were transferred to the Cu mesh by directly wiping the surface of the nanoparticles-deposited GC with the Cu mesh.

3. RESULTS AND DISCUSSION

3.1. Composition and structure of the Pt-Ni and Pt-Co nanoparticles prepared by DPSE

TEM images and size distributions of the $Pt_{93}Ni_7$ and $Pt_{94}Co_6$ nanoparticles are shown in Fig. 2. In both cases spherical particles are observed. The average size and standard deviation of the $Pt_{93}Ni_7$ and $Pt_{94}Co_6$ nanoparticles were 4.4 ± 1.0 nm and 4.0 ± 1.0 nm, respectively.

The Ni or Co content of Pt-Ni or Pt-Co nanoparticles can be controlled by potential applied at the 1st step of the DPSE and $PtCl_6^{2-}$ concentration of the Pt-Ni or Pt-Co baths. Surface and bulk Ni or Co content in the Pt-Ni or Pt-Co nanoparticles prepared at different potentials at the 1st step in DPSE or $PtCl_6^{2-}$ concentrations

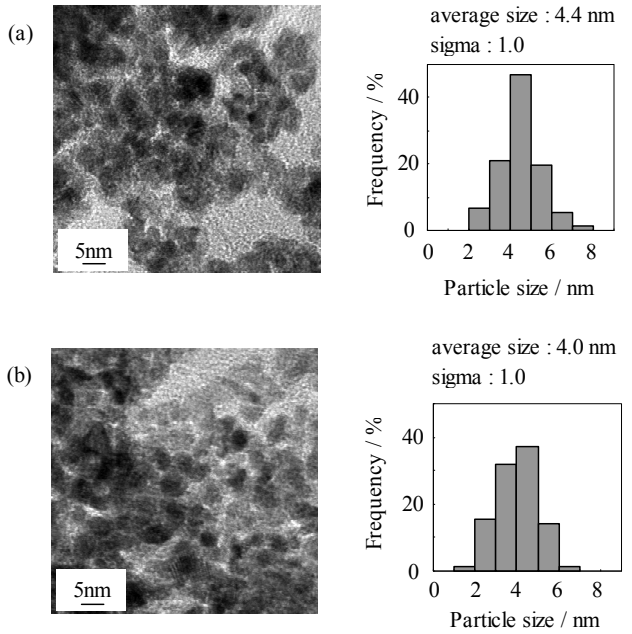

Figure 2. TEM photographs and size distributions of (a) $Pt_{93}Ni_7$ nanoparticles and (b) $Pt_{94}Co_6$ nanoparticles prepared by a cycle of DPSE. Potentials applied at the 1st and 2nd steps were -0.39 V and 0.26 V for the $Pt_{93}Ni_7$ nanoparticles, and -0.44 V and 0.16 V for the $Pt_{94}Co_6$ nanoparticles. The durations of the 2nd step were 10 s in both nanoparticles.

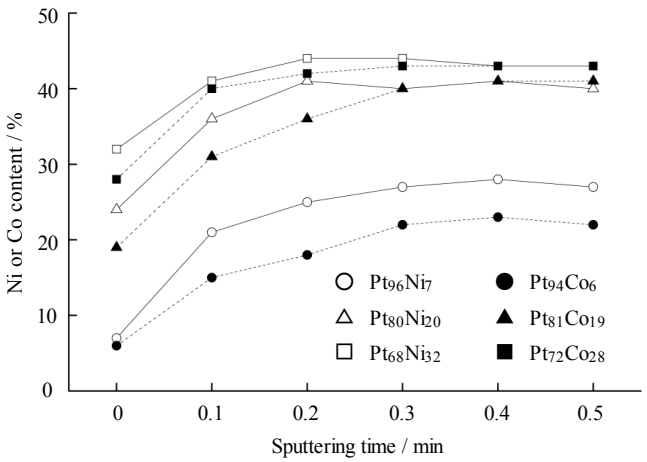

Figure 3. Change in Ni or Co content of the Pt alloy nanoparticles prepared by a cycle of DPSE with Ar^+ sputtering time. Sputtering rate was about 2 nm min^{-1} for oxide layer of SiO_2.

was evaluated by XPS and summarized in Table 1. As the 1st step potential was set at more negative potentials or the$PtCl_6^{2-}$ concentration decreased, the surface Ni and Co contents distinctly increased.

Figure 3 shows change in Ni or Co content with Ar^+ spattering time for Pt-Ni and Pt-Co nanoparticles prepared by a cycle of DPSE. In any composition, the Ni or Co content in the Pt-based alloy nanoparticles was increased with sputtering time, and reached a constant value at a sputtering time of 0.3 min.

Figure 4 shows current-potential (i-E) curves of the $Pt_{93}Ni_7$ and $Pt_{94}Co_6$ nanoparticles-deposited GC electrodes after each step of the 1st cycle of DPSE in an N_2-saturated 0.1 M sulfuric acid solution. The i-E curves in Fig. 4 (a) and (b) are measured with the $Pt_{93}Ni_7$ nanoparticles-deposited GC obtained after the 1st and 2nd steps of DPSE, respectively, and those in Fig. 4 (c) and (d) are measured with the $Pt_{94}Co_6$ nanoparticles-deposited GC obtained after the 1st and 2nd steps of the DPSE, respectively. For comparison, an i-E curve of the Pt nanoparticles-deposited GC is shown in Fig. 4 (e). The i-E curve has typical redox waves due to adsorption and desorption of atomic hydrogen on Pt in the potential range below 0.3 V.

In Fig. 4 (a) and (c), at the 1st sweep a large oxidation peak was observed in the potential range below 0.3 V, while at the 2nd sweep it decreased, suggesting that the surface Ni of $Pt_{93}Ni_7$ nanoparticles or surface Co of $Pt_{94}Co_6$ nanoparticles dissolved out during the 1st sweep. On the other hand, in Fig. 4 (b) and (d) such a decrease in oxidation peak was not observed. This indicates that the surface Ni or Co component of the $Pt_{93}Ni_7$ or $Pt_{94}Co_6$ nanoparticles has com-

Table 1. The preparation conditions and transition metal contents of the Pt and Pt alloy nanoparticles measured by XPS.

	Solutions	Step potentials and duration of DPSE				Transition metal contents of Pt alloy nanoparticles	
	$PtCl_6^-$ concentration	1st step Potential (vs. RHE)	1st step duration (s)	2nd step Potential (vs. RHE)	2nd step duration (s)	measured by XPS (surface)	measured by XPS (after 0.3min sputtering)
Pt-Ni	20 mM	-0.39 V	5	0.26 V	10	7	27
	2.5 mM	-0.44 V			10	20	40
	1.25 mM	-0.59 V			30	32	44
Pt-Co	20 mM	-0.44 V	5	0.16 V	10	6	22
	5.0 mM	-0.44 V			10	19	40
	2.5 mM	-0.54 V			30	28	43
Pt	2.5 mM	-0.44 V	5	0.26 V	10	-	-

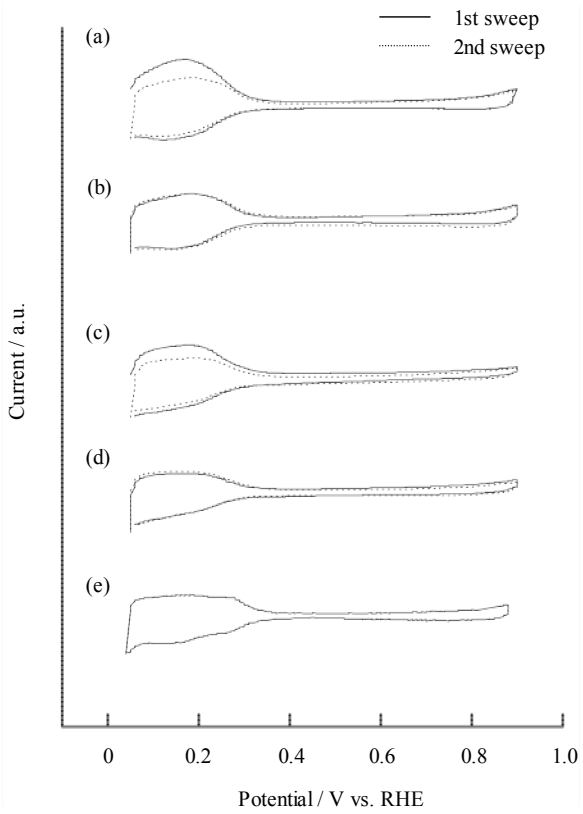

Figure 4. Current density-potential (i-E) curves of the Pt alloy and Pt nanoparticles-deposited GC electrodes in an N_2-saturated 0.1 M sulfuric acid solution. Solid and dotted curves show curves at the 1st and 2nd sweeps, respectively. Sweep rate was 20 mV s^{-1}.
(a) $Pt_{93}Ni_7$ nanoparticles-deposited GC electrode after the 1st step of DPSE. (b) $Pt_{93}Ni_7$ nanoparticles-deposited GC electrode after the 2nd step of DPSE. (c) $Pt_{94}Co_6$ nanoparticles-deposited GC electrode after the 1st step of DPSE. (d) $Pt_{94}Co_6$ nanoparticles-deposited GC electrode after the 2nd step of DPSE. (e) Pt nanoparticles-deposited GC electrode.

pletely dissolved out during the 2nd step of the DPSE.

As Fig. 3 demonstrates, in any composition, the surface Ni or Co content in the Pt-based alloy nanoparticles is increased with sputtering time, and reaches a constant value at a sputtering time of 0.3 min. Judging from the sputtering rate, the sputtering time of 0.3 min is broadly estimated to be thickness of 0.6 nm. Considering that the escape depth of photoelectrons from the surface is about 1 nm [21], the Ni or Co content of the thin surface layer of $Pt_{93}Ni_7$ or $Pt_{94}Co_6$ nanoparticles with the particle size of 4.4 or 4.0 nm should be much less than their bulk content.

To evaluate the total Ni or Co content of the Pt-based alloy nanoparticles, it was measured by ICPS. For example, the total Ni and Co contents of $Pt_{93}Ni_7$ and $Pt_{94}Co_6$ were evaluated to be 30 and 26 %, respectively. Meanwhile the Ni and Co contents of $Pt_{93}Ni_7$ and $Pt_{94}Co_6$ evaluated by XPS were 7 and 6 %, respectively. The total Ni and Co contents are much higher than those determined by XPS, indicating that the Pt is enriched near the surface of the nanoparticles. This also means that XPS is available for evaluating

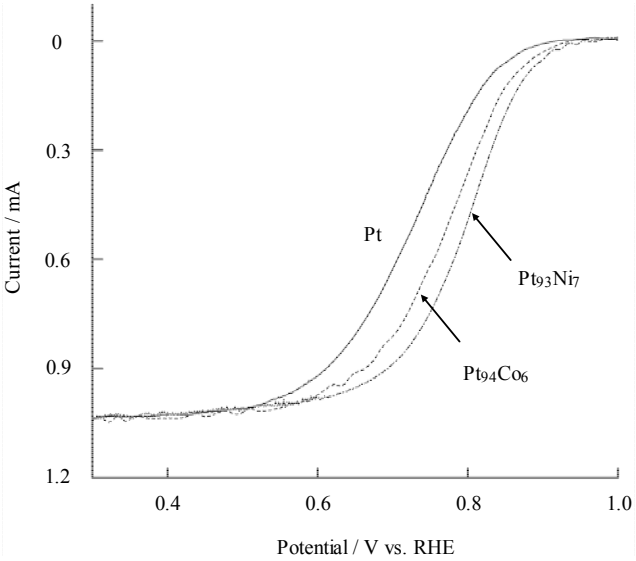

Figure 5. Hydrodynamic voltammograms for ORR on $Pt_{93}Ni_7$, $Pt_{94}Co_6$, and Pt nanoparticles-deposited GC electrodes at a rotation speed of 1600 rpm in an O_2 saturated 0.1M sulfuric acid solution. Each nanoparticle was prepared by a cycle of DPSE. Sweep rate was 1 mV s^{-1}.

the Ni and Co contents near the surface in this study. In addition, as shown in Fig. 4 (b) and (d), both Pt-Ni and Pt-Co nanoparticles after the 2nd step of DPSE electrochemically behaved just like the Pt nanoparticles (Fig. 4 (e)). Therefore, it is likely that a very thin Pt layer, that is, a Pt skin layer is formed on the surface of Pt-Ni or Pt-Co nanoparticles during a cycle of DPSE.

3.2. ORR activity of the Pt-Ni and Pt-Co nanoparticles prepared by the DPSE

Hydrodynamic voltammograms at a rotation speed of 1600 rpm of the Pt-Ni and Pt-Co nanoparticles-deposited GC electrodes in O_2-saturated 0.1M H_2SO_4 are shown in Fig. 5. The Koutecky-Levich plots obtained at different rotation speeds were drawn, and each plot had linear relationship between measured current $(i)^{-1}$ and $\omega^{-1/2}$, and kinetically controlled current (i_k) was evaluated from the inverse of the intercept at $\omega^{-1/2} = 0$ for each plot. Specific activity

Table 2. Specific Activity (SA) at 0.8 V on Pt-Ni, Pt-Co, and Pt nanoparticles-deposited GC.

	Specific Activity (SA)
	mA cm^{-2} at 0.8 V
$Pt_{93}Ni_7$	0.79
$Pt_{76}Ni_{24}$	0.56
$Pt_{68}Ni_{32}$	0.47
$Pt_{94}Co_6$	0.71
$Pt_{81}Co_{19}$	0.53
$Pt_{72}Co_{28}$	0.65
Pt	0.49

(SA) for ORR is defined as i_k per real surface area at 0.8 V (vs. RHE). The SA values of the Pt-Ni and Pt-Co nanoparticles with various compositions are shown in Table 2. The Pt-Ni and Pt-Co nanoparticles had higher SA than the Pt nanoparticles. Among three kinds of Pt-Ni or Pt-Co nanoparticles-deposited GC, the lower the Ni or Co content was, the higher the SA value was. This result seems to contradict to the result by Toda et al. [8], who described that the maximum activity was obtained at ca. 30 and 40 % bulk contents of Ni or Co, respectively. However, even though the surface contents were very low in our research, the bulk contents of Pt-Ni and Pt-Co nanoparticles were also ca. 30 ~ 40 %, as shown in Table 1. Therefore, the result obtained here on the relationship between the bulk content and ORR activity is in agreement with Toda's result.

The improvement in ORR activity of the Pt-based alloy is ascribable to the increased d-electron vacancy of Pt atom on the surface layer caused by underlying alloy [8]. In principle, the increase in d-electron vacancy shifts the Pt $4f_{7/2}$ and Pt $4f_{5/2}$ peaks in the XPS spectra toward higher binding energies, while the Pt 4f peaks of the present Pt-Ni and Pt-Co nanoparticles showed a slight shift (0.1 ~ 0.3 eV) toward higher binding energies, implying that the d-electron vacancy of the surface Pt increased in the present case. So far, there have been some papers on the relationship between d-orbital vacancy or composition and ORR activity [8, 22], and the volcano type correlation has been proposed. However, the direct relationship between the XPS peak shift and the ORR activity has not been clear. The XPS data is average value of the surface of about 1nm thickness, so it does not reflect only the electronic structure of first layer of the nanoparticles on which oxygen reduction occurs. Therefore the XPS peak shift may not be directly connected to the ORR activity. The details of the mechanism for ORR improvement are still unclear, so we need to allow for other factors to explain the high ORR activity of those alloy particles.

3.3. Corrosion resistance and stability of the Pt-Ni and Pt-Co nanoparticles by the DPSE

For evaluating the stability and corrosion resistance of the Pt-Ni and Pt-Co nanoparticles-deposited GC electrodes, the repetitive potential cycling was conducted in the potential range from 0.05 to 1.2 V in an N_2-saturated 0.1M sulfuric acid solution. It should be noted that Ni or Co dissolves in the potential range below 0.45V and Pt dissolves in the potential range above 0.8 V [23, 24], and in addition, the sintering of Pt particles occurs in the potential range below 0.75 V [25]. Therefore, the repetitive potential cycling should be a severe test atmosphere to metamorphose the Pt-Ni and Pt-Co alloy nanoparticles.

Figure 6 (a), (b), and (c) show cyclic voltammograms (CV) measured at the 10th, 100th, 700th, and 1000th cycles of potential cycling with Pt, $Pt_{93}Ni_7$, and $Pt_{94}Co_6$ nanoparticles-deposited GC electrodes, respectively. All the nanoparticles were prepared by DPSE in which the potential applied at the 1st and 2nd steps were -0.44 and 0.26 V for the Pt nanoparticles, -0.39 and 0.26 V for the Pt-Ni nanoparticles, and -0.44 and 0.16 V for the Pt-Co nanoparticles, respectively. In Fig. 6 (a), the peaks at potentials more negative than 0.3 V due to the adsorption and desorption of atomic hydrogen on Pt got smaller with an increase in the number of potential cycling, indicating clearly the loss of the surface area. The surface area loss has been ascribed to the dissolution / redeposition

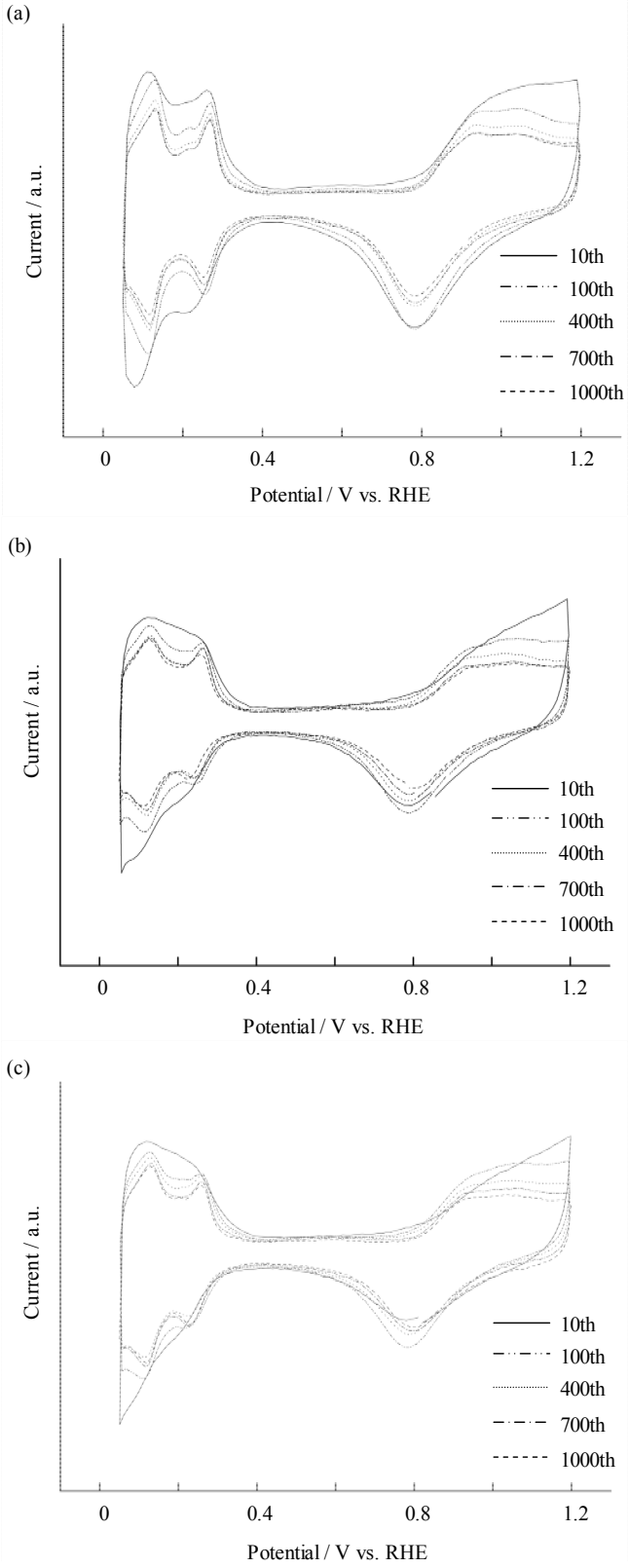

Figure 6. Cyclic voltammograms of (a) Pt, (b) $Pt_{93}Ni_7$, and (c) $Pt_{94}Co_6$ nanoparticles-deposited GC electrodes in an N_2-saturated 0.1 M sulfuric acid solution. Each nanoparticle was prepared by a cycle of DPSE. Sweep rate was 100 mV s^{-1}.

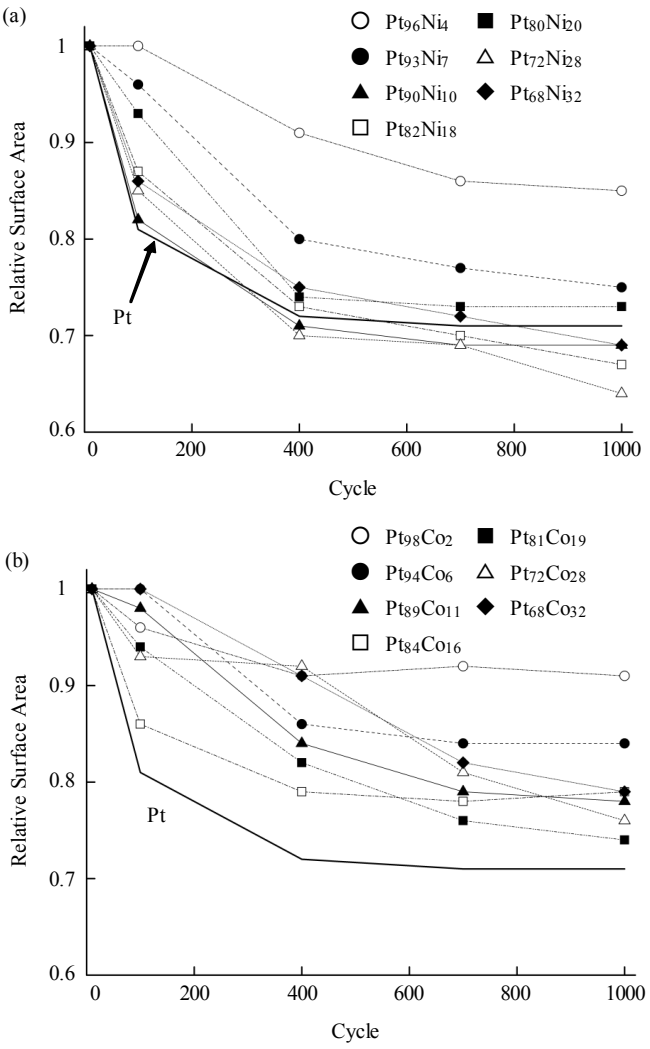

Figure 7. Relative surface areas as a function of the cycle number for the (a) Pt-Ni and (b) Pt-Co nanoparticles-deposited GC. Each nanoparticles were prepared by a cycle of DPSE. The relative surface area is determined with the reference to the real surface area at the 10th cycle. The heavy line in each graph shows the curve for the Pt nanoparticles-deposited GC. The durations of the 2nd step for preparing $Pt_{72}Ni_{28}$, $Pt_{68}Ni_{32}$, $Pt_{72}Co_{28}$, and $Pt_{68}Co_{32}$ were 30 s, and the rest, 10 s.

and the sintering of Pt nanoparticles [22-24]. Even in case of the $Pt_{93}Ni_7$ and $Pt_{94}Co_6$ nanoparticles as shown in Fig. 6 (b) and (c), the surface area loss was observed with an increase in the number of potential cycling, but it looked smaller than that for the Pt nanoparticles.

Relative surface areas of the Pt-Ni and Pt-Co nanoparticles with different compositions at various cycle numbers were measured and summarized in Fig. 7 (a) and (b), respectively. Each relative surface area was defined as a ratio of the real surface area at each cycle number to that at 10th cycle.

For any Pt-based alloy nanoparticles, the relative surface area was decreased within a few hundred potential cycles and subsequently became constant. The lower the surface Ni or Co content was, the lower the decrease rate of relative surface area was. In addition, the decrease rate of relative surface area for the Pt-Co nanoparticles was lower than that for the Pt-Ni nanoparticles. Especially in case of 2 % Co content, the decrease rate was so low that its relative surface area was kept more than 90% even after 1000 potential cycles.

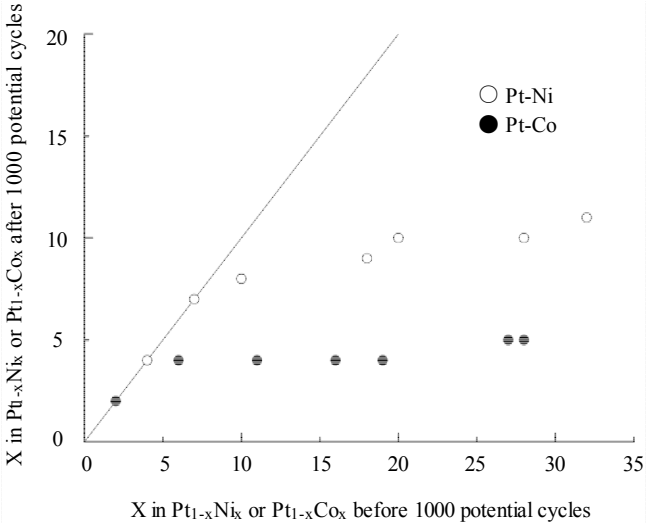

Figure 8. Changes in transition metal contents of Pt-Ni and Pt-Co nanoparticles by 1000 potential cycles as a function of (○) the surface Ni contents of the Pt-Ni nanoparticles and (●) the surface Co contents of Pt-Co nanoparticles. Each nanoparticle was prepared by a cycle of DPSE.

Figure 8 shows the surface Ni or Co content in the Pt-based alloy nanoparticles after the 1000 potential cycles plotted against that before the potential cycling. When the surface Ni or Co content before potential cycling was less than about 8 % Ni for the Pt-Ni nanoparticles or less than about 4 % Co for the Pt-Co nanoparticles, the plots were on the straight line with gradient = 1, indicating that the surface Ni or Co content was unchanged even after the 1000 potential cycling.

When the surface Ni or Co content before the potential cycling was higher than 8 % Ni or 4 % Co, the plots deviated from the straight line and reached a constant value, indicating that the Ni or Co dissolves out from the Pt-alloy nanoparticles depending on its content.

In most reports on the deterioration of Pt-based alloy catalysts, the surface transition metals was not detected by XPS measurement after the deterioration test [8, 9]. However, in the present case, the surface Ni or Co component were detected even after the potential cycling test. The fact clearly indicates that the transition metal components of nanoparticles prepared by DPSE are tightly held in the skin layer.

It is generally believed that Pt is stabilized by alloying with transition metals [12, 16]. Greeley et al. [15] reported that a Pt skin layer on Pt-based alloys is more stable than pure Pt by thermodynamical calculation using density functional theory. In their research, on the Pt alloy nanoparticles with low surface transition

metal content such as $Pt_{96}Ni_4$ and $Pt_{98}Co_2$, the decrease rate of the relative surface area was lower than Pt (Fig. 7). These nanoparticles exhibited no leaching of transition metal even after potential cycling (Fig. 8). Therefore, there was no effect of transition metal leaching on the surface area loss. These results also confirm the existence of the stable Pt skin layer on the Pt-based alloys.

In addition, after the 1000 potential cycles, hydrodynamic voltammograms of the Pt-Ni and Pt-Co nanoparticles-deposited GC electrodes were measured and the SA values at 0.8 V for nanoparticles with the surface compositions of $Pt_{93}Ni_7$ and $Pt_{94}Co_6$ were evaluated. The SA values of the $Pt_{93}Ni_7$ and $Pt_{94}Co_6$ nanoparticles after the 1000 potential cycles were 0.64 and 0.57 mA cm^{-2}, respectively, and a little decreased compared to the initial (Table 2). But both alloy nanoparticles maintained higher performance than the Pt nanoparticles. The Pt 4f peaks of the $Pt_{93}Ni_7$ and $Pt_{94}Co_6$ nanoparticles after 1000 potential cycles also shifted slightly toward higher binding energies than those of Pt nanoparticles. The degree of peak shift of nanoparticles after 1000 potential cycles was also the same with that before 1000 potential cycles. As mentioned above, the degree of Pt 4f shift does not always depend on the degree of d-electron vacancy. However, the peak shift was observed actually, suggesting the electronic structure of surface Pt has changed, therefore, the nanoparticles even after 1000 potential cycles exhibited higher ORR performance.

4. CONCLUSION

(i) The Pt-Ni and Pt-Co nanoparticles covered with a Pt skin layer could be prepared by the DPSE. With this method, the composition and size were to be controlled in one process. The Pt-Ni and Pt-Co nanoparticles by the DPSE exhibited higher ORR activity, corrosion resistance, and stability than Pt nanoparticles, suggesting that Pt-skin layer was effective on the improvements of them.

(ii) The corrosion resistance and stability varied according to the surface composition of the Pt-Ni and Pt-Co nanoparticles, the nanoparticles of low surface Ni or Co content showed good performances. Especially in case of 2 % surface Co content in the Pt-Co nanoparticles, the surface area was maintained to be more than 90 % and the loss of Co was not occurred even after the deterioration test. That is, there has a strong correlation between the corrosion resistance and stability.

(iii) A Pt-skin layer on the Pt-Ni or Pt-Co nanoparticles by the DPSE was stabilized because the Pt-skin layer was alloyed with Ni or Co. Comparing the Pt-Ni and Pt-Co, the Pt-Co was more stable, that is, the Pt-Co was formed more stable Pt-skin layer.

REFERENCES

[1] S. Mukerjee, S. Srinivasan, M. P. Soriaga, J. McBeen, J. Phys. Chem., 99, 4577 (1995).

[2] U.A. Paulus, A. Wokaum, G.G. Scherer, T.J. Schmidt, V. Stamenkovic, V. Radmilovic, N.M. Markovic, P.N. Ross, J. Phys. Chem., B 106, 4181 (2002).

[3] H. Yang, W. Vogel, C. Lamy, N. Alonso-Vante, J. Phys. Chem., B 108, 11024 (2004).

[4] L. Xiong, A. Manthiram, J. Electrochem. Soc., 151, A1507 (2004).

[5] T. P. Moffat, J. J. Mallett, Sun-Mi Hwang, J. Electrochem. Soc., 156, B238 (2009).

[6] S. Koh, M.F. Toney, P. Strasser, Electrochim. Acta, 52, 2765 (2007).

[7] V. Jalan, E.J. Taylor, J. Electrochem. Soc., 130, 2299 (1983).

[8] T. Toda, H. Igarashi, H. Uchida, M. Watanabe, J. Electrochem. Soc., 146, 3750 (1999).

[9] A. Bonkdarpour, J. Wenzel, D.A. Stevens, S. Sheng, T.L. Monchesky, R Löbel, R.T. Atanasoski, A.K. Schmoeckel, G.D. Vernstorm, M.K. Debe, J.R. Dahn, J. Electrochem. Soc., 152, A61 (2005).

[10]N. Wakabayashi, M. Takeichi, H. Uchida, M. Watanabe, J. Phys. Chem., B 109, 5836 (2005).

[11]H.R. Colon-Mercado, B.N. Popov, J. Power Sources, 155, 253 (2006).

[12]N. Travitsky, T. Ripenbein, D. Golodnitsky, Y. Rosenberg, L. Burshtein, E. Peled, J. Power Sources, 161, 782 (2006).

[13]S.C. Zignani, E. Antolini, E.R. Gonzalez, J. Power Sources, 191, 344 (2009).

[14]V. Stamenkovic, B.S. Mun, K.J.J. Mayrhofer, P.N. Ross, N.M. Markovic, J. Am. Chem. Soc., 128, 8813 (2006).

[15]J. Greeley, J.K. Norskov, Electrochim. Acta, 52, 5829 (2007).

[16]J.R. C. Salgado, E. Antolini, R. Gonzalez, J. Phys. Chem., B 108, 17767 (2004).

[17]V. Stamenkovic, T.J. Schmidt, P.N. Ross, N.M. Markovic, J. Phys. Chem., B106, 11970 (2002).

[18]A. Tegou, S. Papadimitriou, E. Pavlidou, G. Kokkinidis, S. Sotiropoulos, J. Electroanal. Chem., 608, 67 (2007).

[19]J. Zhang, F.H.B. Lima, M.H. Shao, K. Sasaki, J.X. Wang, J. Hanson, R.R. Adzic, J. Phys. Chem., B109, 22701 (2005).

[20]T. Nishimura, T. Morikawa, M. Yokoi, C. Iwakura, H. Inoue, Electrochim. Acta, 54, 499 (2008).

[21]C.R. Brundle, J. Vac. Thecnol., 11, 212 (1974).

[22]S. Mukerjee, S. Srinivasan, M.P. Soriaga, J. McBreen, J. Electrochem. Soc., 142, 1409 (1995).

[23]P. Bindra, S.J. Clouser, E. Yeager, J. Electrochem. Soc., 126, 1631 (1979).

[24]A. Honji, T. Mori, K. Tamura, Y. Hishimura, J. Electrochem. Soc., 135, 355 (1988).